Fast RT Model for SSMIS Upper-air Sounding Channels

Yong Han
NOAA/NESDIS/STAR

ITSC-15
Maratea, Italy
4-10 October 2006

Outline

- Radiometric characteristics of SSMIS channels 19-14

  - Zeeman effect
  - Channel passbands
  - Weighting function variations with the Earth's magnetic field
  - Radiance variations with the Earth's magnetic field
  - A case study of Zeeman effect on channel 20

- Fast RT model

  - Algorithm
  - Model tests against line-by-line models
  - Model results compared with measurements

- Summary and conclusions

Zeeman Effect

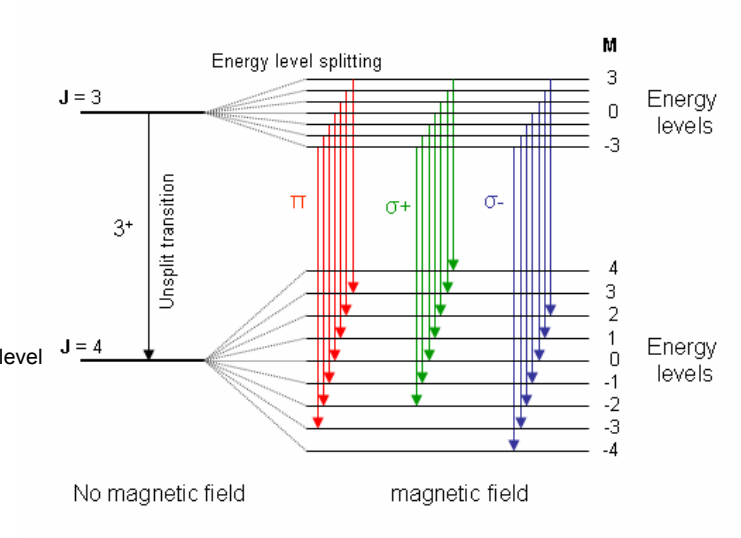

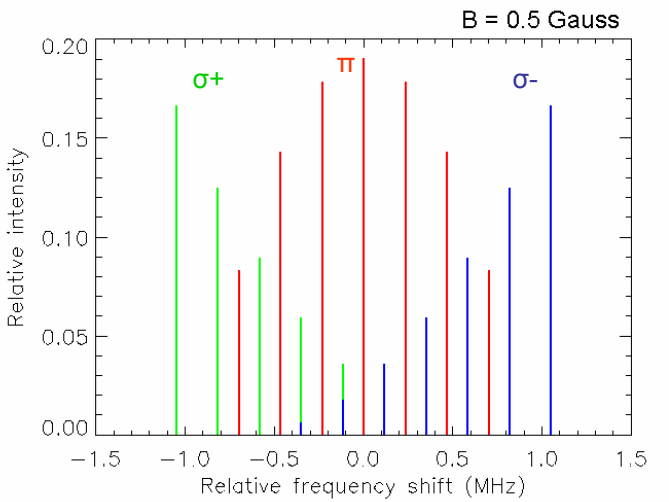

Zeeman spectral splitting of the 3^+ O2 line (unsplit frequency: 58.446590 GHz)

Energy level splitting:

In the presence of an external magnetic field, each energy level associated with the total angular momentum quantum number J is split into 2J+1 levels corresponding to the azimuthal quantum number M = -J, …, 0, …,J

Transition lines (Zeeman components) :

The selection rules permit transitions with $\Delta J = \pm 1$ and $\Delta M = 0, \pm 1$. For a change in J (i.e. J=3 to J=4, represented by 3^+), transitions with

$\Delta M = 0$ are called π components,
$\Delta M = 1$ are called σ+ components and
$\Delta M = -1$ are called σ- components.

Polarization:

The three groups of Zeeman components also exhibit polarization effects with different characteristics. Radiation from these components received by a circularly polarized radiometer such as the SSMIS upper-air channels is a function of the magnetic field strength $|\mathbf{B}|$, the angle θ_B between **B** and the wave propagation direction **k** as well as the state of atmosphere, not dependent on the azimuthal angle of **k** relative to **B**.

SSMIS upper-air channel parameters

Ch #	Passband 1		Passband 2		Passband 3		Passband 4	
	F_0 (GHz)	BW (MHz)	F_0 (GHz)	BW (MHz)	F_0 (GHz)	BW (MHz)	F_0 (GHz)	BW (MHz)
19	62.9980	1.34	63.5685	1.36				
20	60.4348	1.34	61.1506	1.37				
21	60.4328	1.26	60.4368	1.23	61.1486	1.33	61.1526	1.33
22	60.4293	2.62	60.4403	2.61	61.1451	2.66	61.1561	2.67
23	60.4188	7.01	60.4508	7.17	61.1346	7.40	61.1666	7.44
24	60.3848	26.63	60.4848	26.33	61.1006	26.04	61.2006	26.88

All the six channels are left-circular polarization

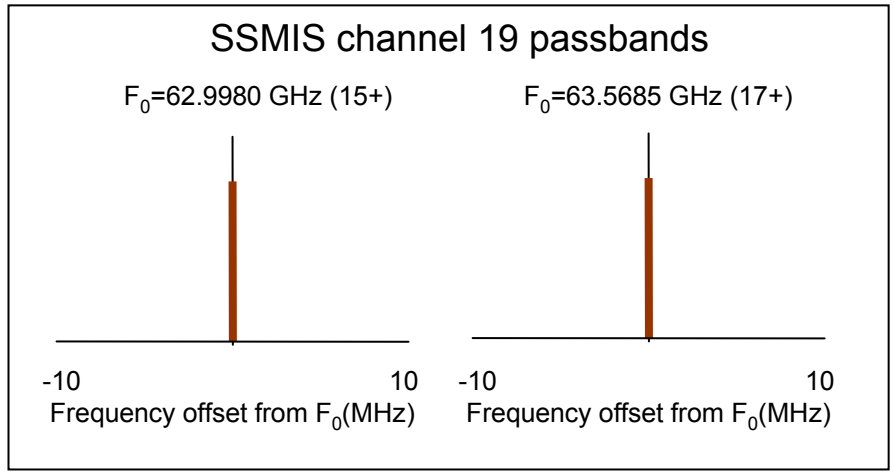

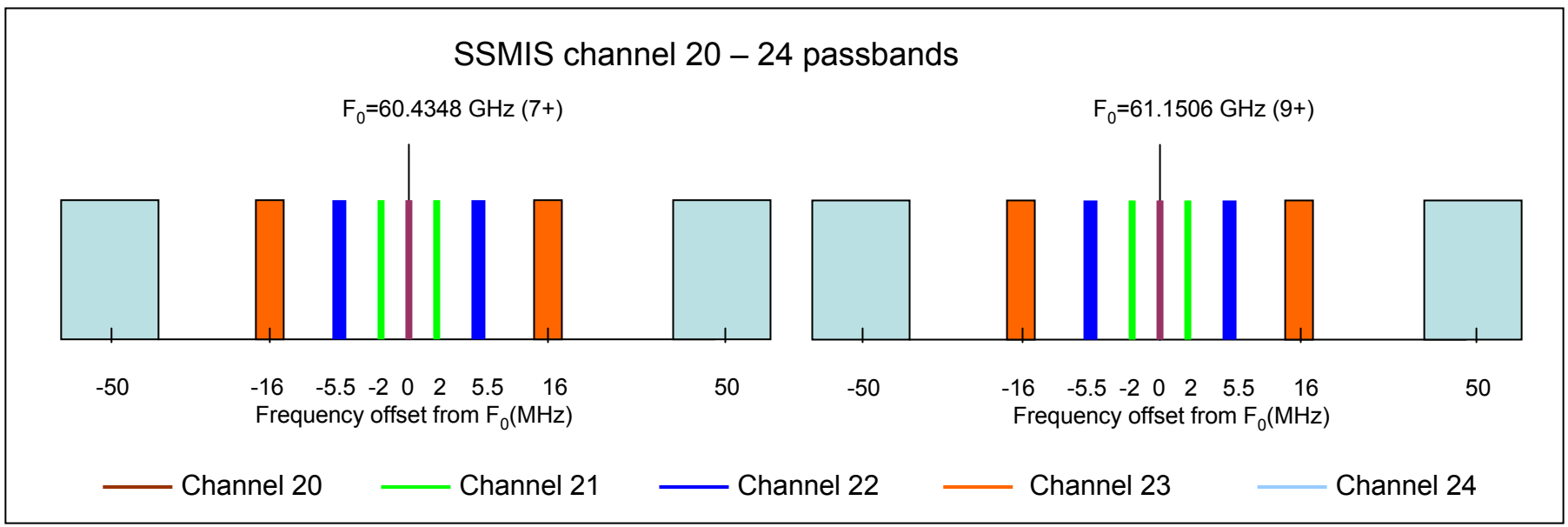

- The passbands of channels 19 and 20 are centered at the O2 rotational transition line 7+, 9+, 15+ or 17+.
- The paired passbands of channels 21 – 24 are located with equal distances from the center of the transition line 7+ or 9+.

Variation of the Earth's magnetic field

Field strength

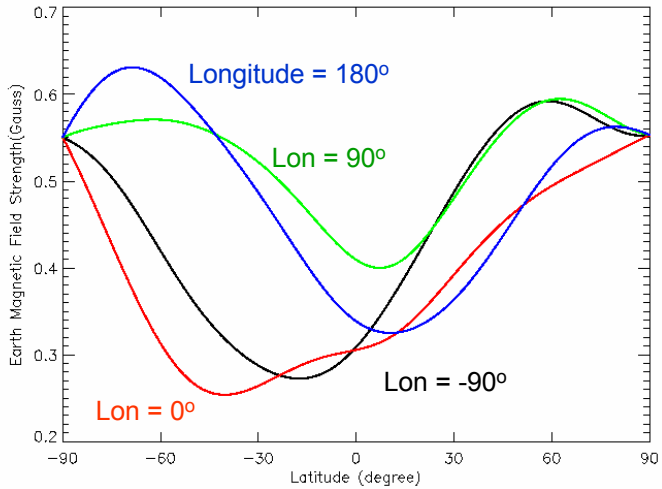

Horizontal direction from North (east +)

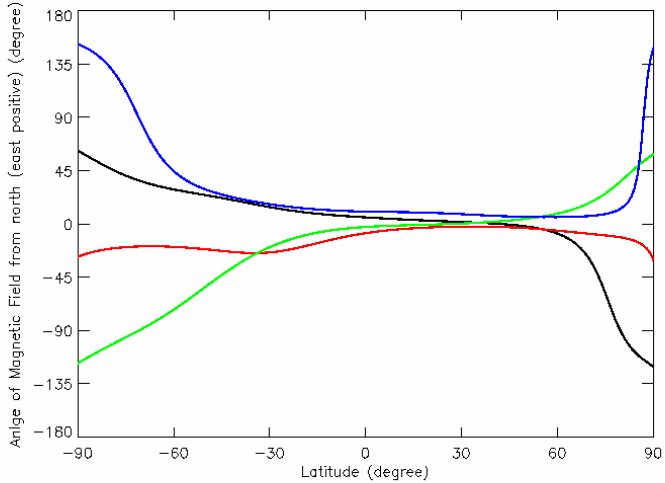

Field zenith angle

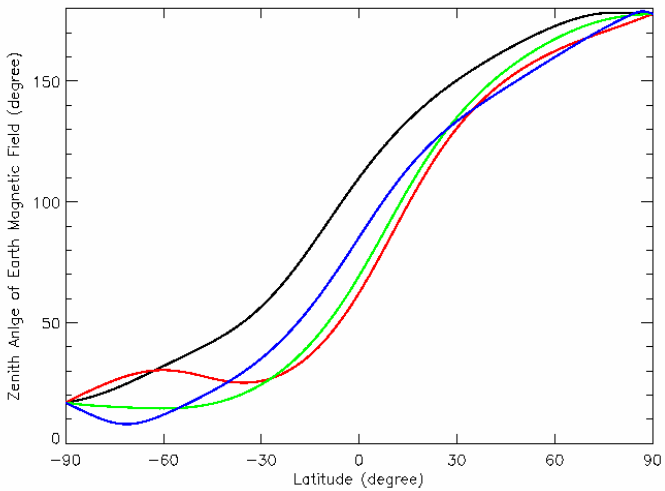

Field strength at different heights

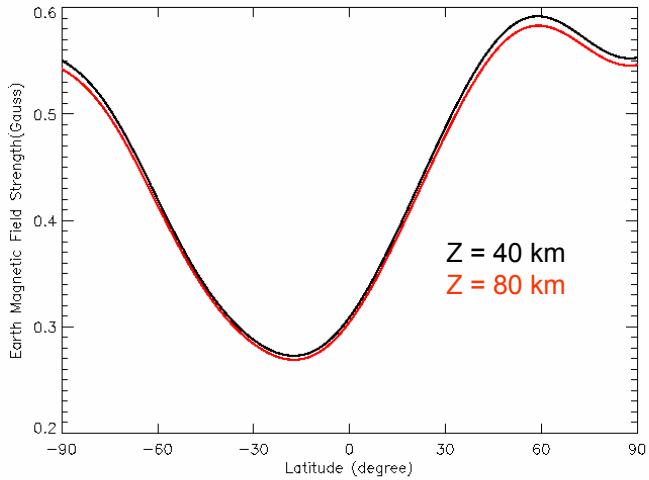

The field may be treated as a constant with height

The magnetic field was computed with IGRF

Radiometric characteristics of channel 19 – 24 (1)

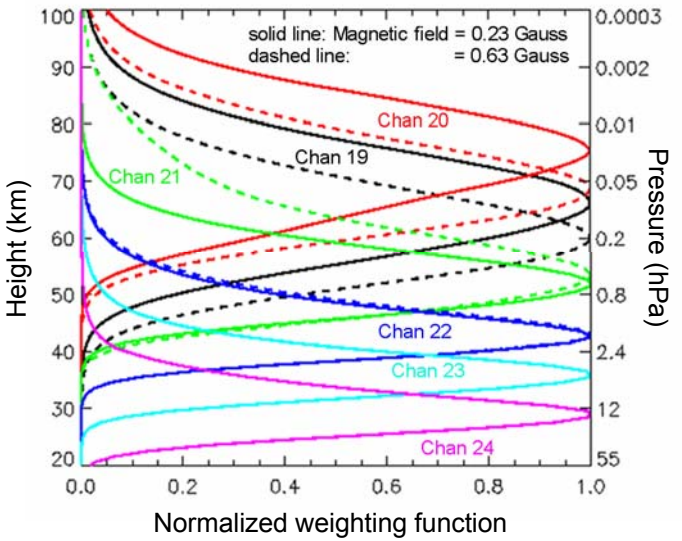

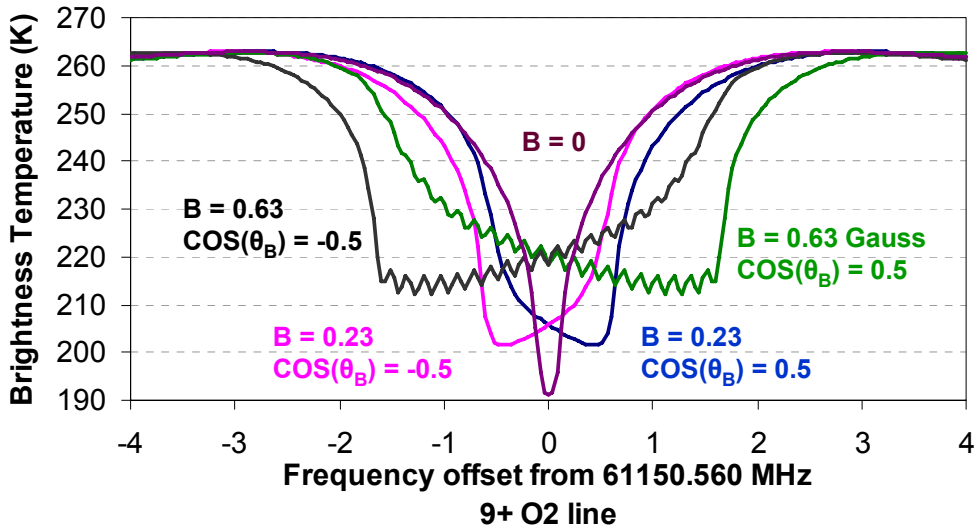

- The weighting function peak heights of channels 19 and 20 decrease when the magnetic field strength increases because the two channels are centered at the transition lines, where the absorption decreases.
- The weighting function peak heights of channels 21 and 22 increase when the magnetic field strength increases since the channels are located off the transition line centers, in the places where the absorption increases.
- The channel brightness temperatures do not depend on the sign of $COS(\theta_B)$, if the central frequencies of the passbands in channels 19 and 20 are centered at the transition lines and each symmetric pair of the passbands in channels 21 – 24 have approximately the same bandwidth. (see also slide 10)

Radiometric characteristics of channel 19 – 24 (2)

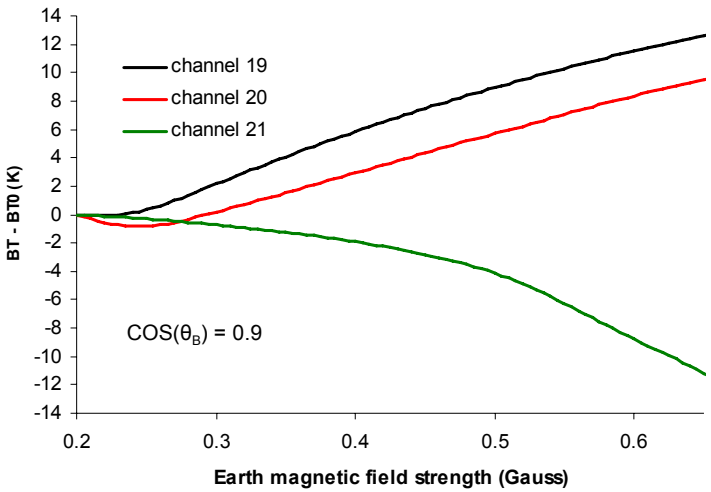

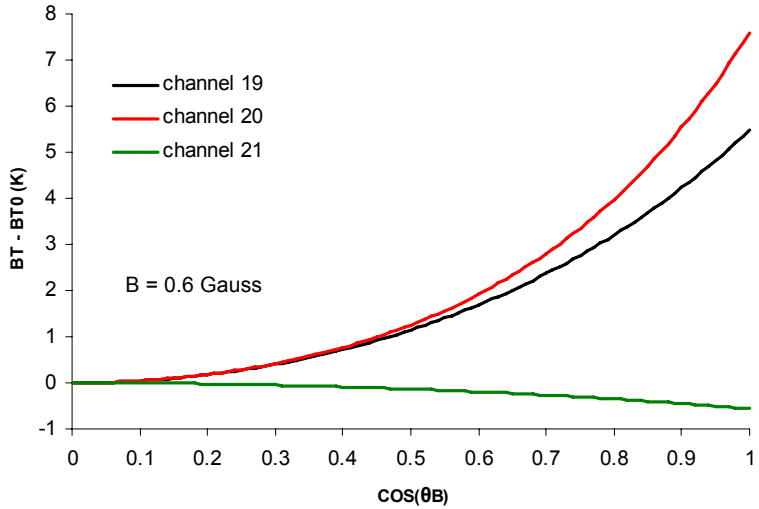

BT_0 – brightness temperature offset, channel dependent

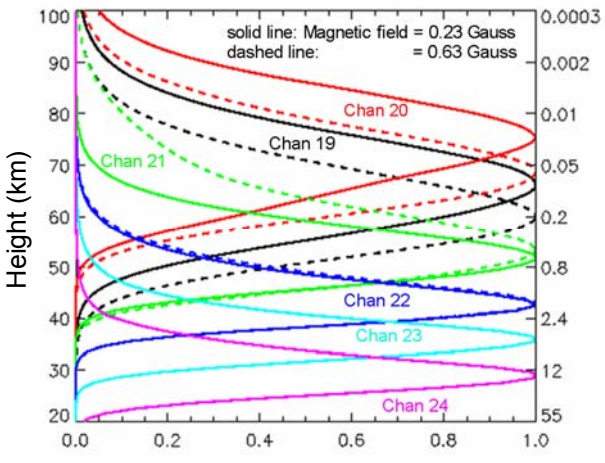

US Standard atmosphere (1976)

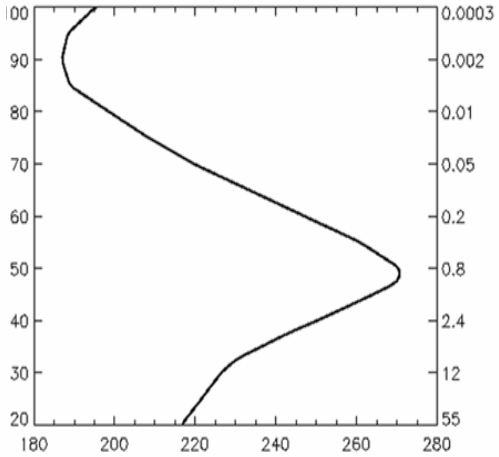

- The brightness temperatures increase with the Earth's magnetic filed strength in channels 19 and 20 because the weighting function peak heights decrease and move into areas with warmer air temperature.
- Channel 21 is in a opposite situation.
- The variations of the brightness temperature with $COS(\theta_B)$ can be explained similarly.

Radiance measurements plotted as functions of magnetic field strength and COS(θ_B)

Channel 19 Channel 20 Channel 21

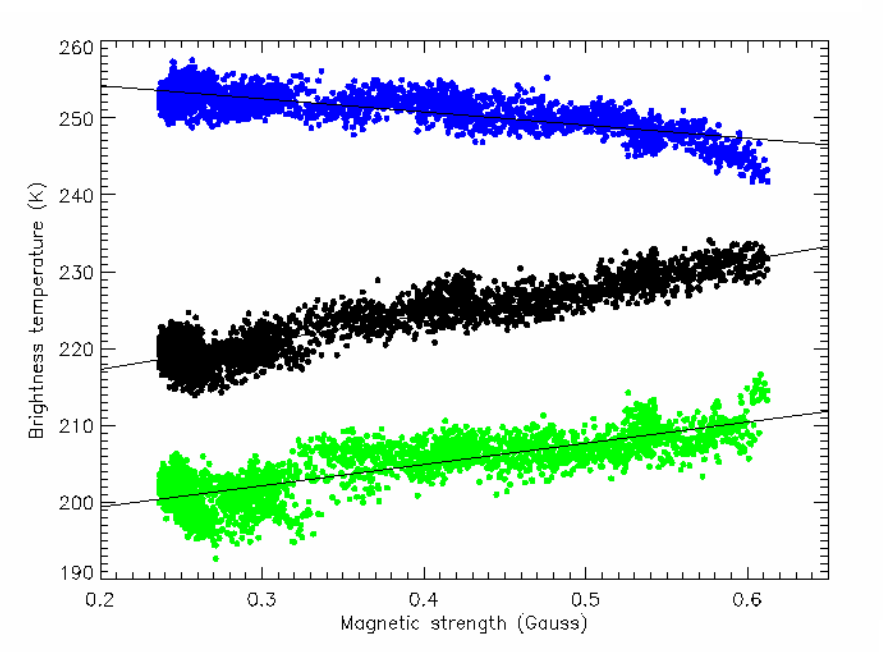

$0.8 < |COS(\theta_B)| < 1.0$

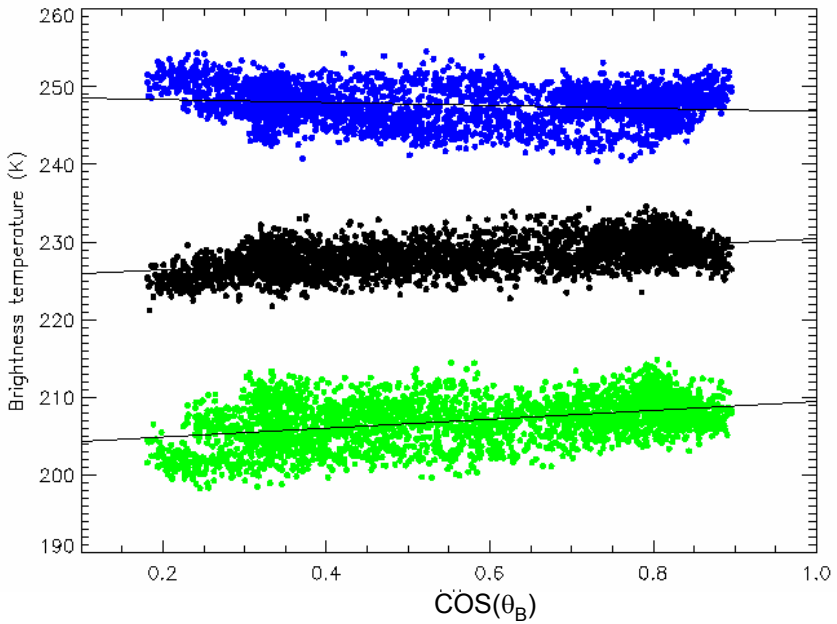

$0.5 < B < 0.6$ Gauss

Data were taken on February 15, 2006 within latitude range between 40S and 50S

Radiometric characteristics of channel 19 – 24 (3)

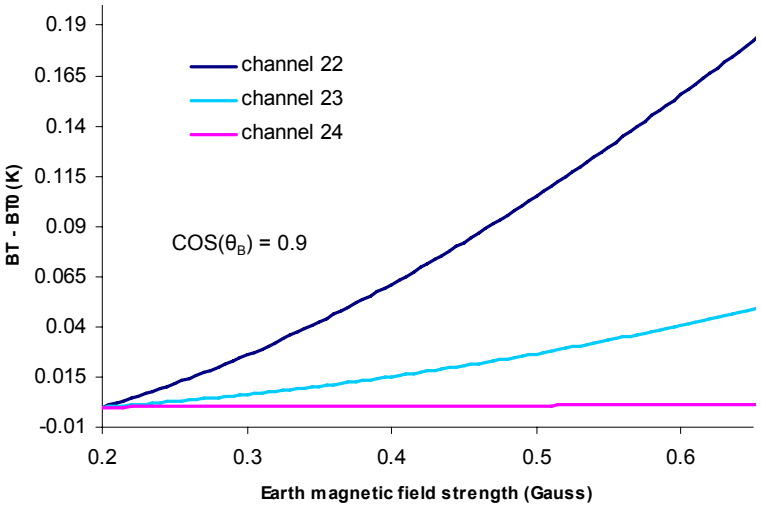

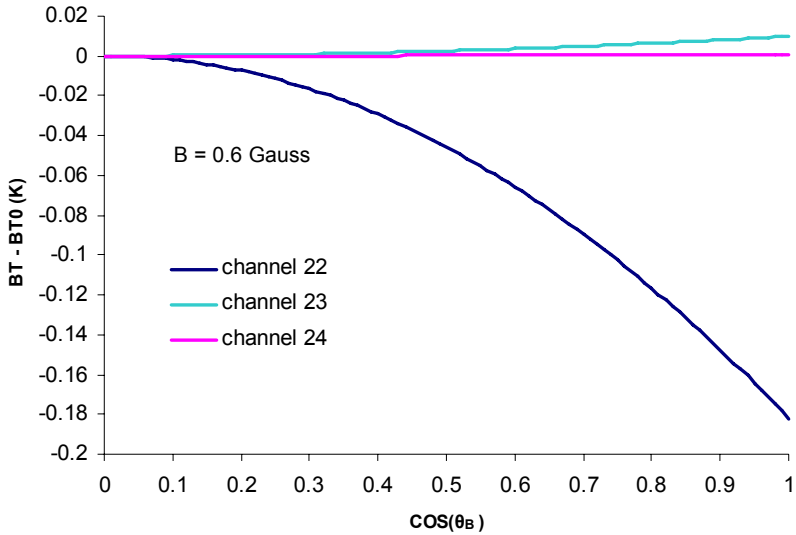

Channel 24 is not affected by Zeeman-splitting

Radiometric characteristics of channel 19 – 24 (4)

The effect of shifting passbands by about 0.03 MHz in channel 20: the channel shows a dependence on the sign of the cosine angle between the Earth's magnetic field and wave propagation direction

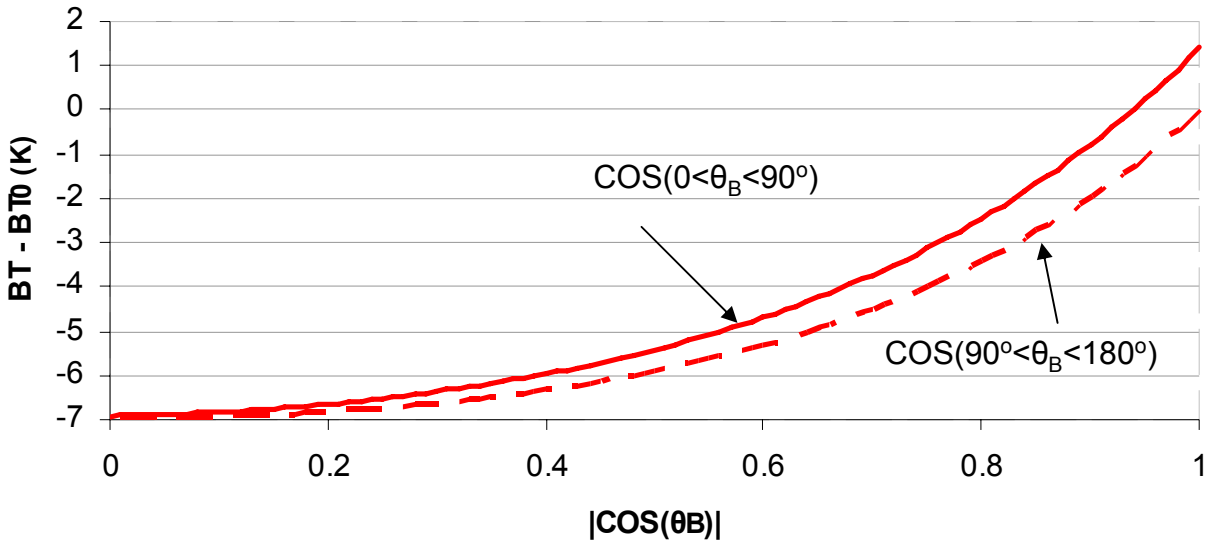

Zeeman effect case study: measurement simulations along a track of channel-20 observations (1)

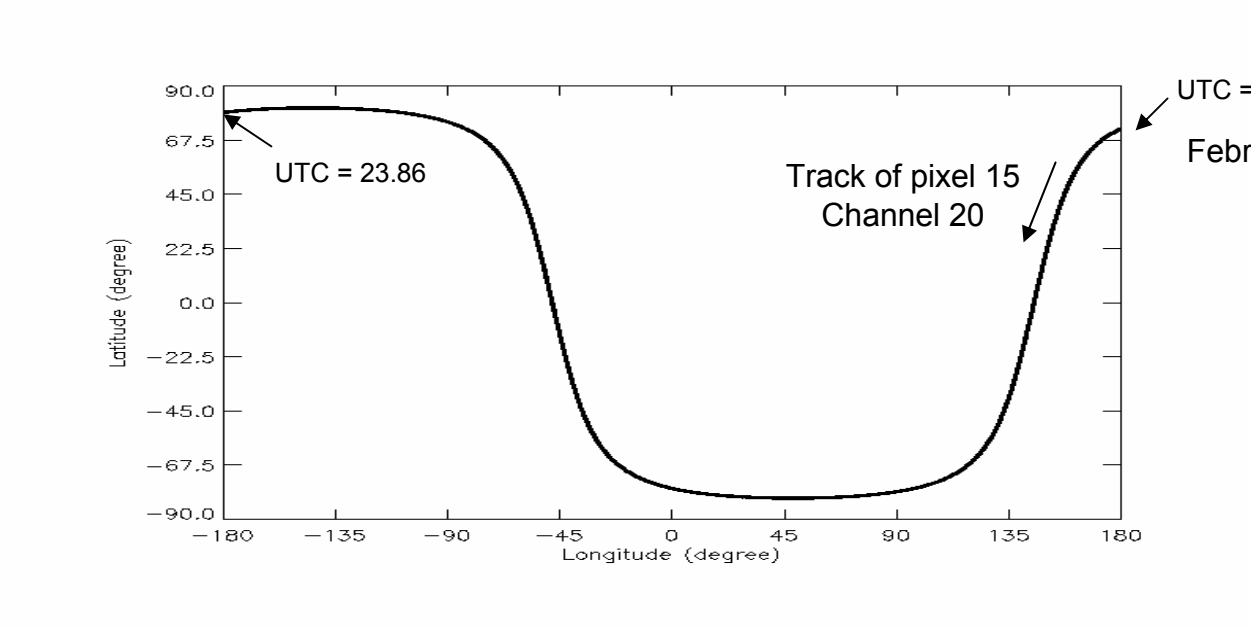

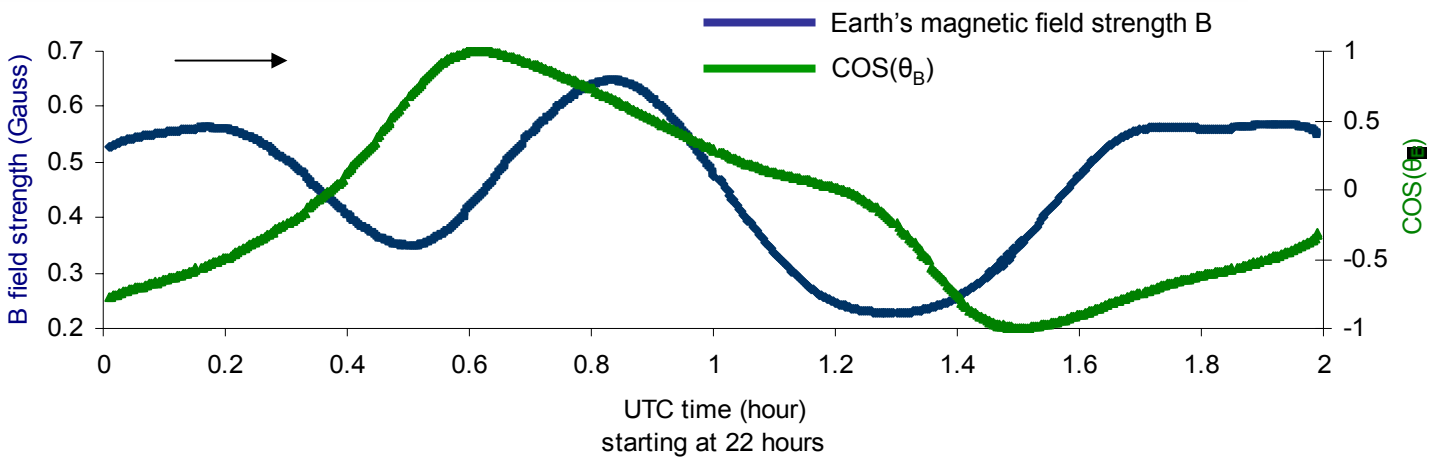

Zeeman effect case study: measurements and simulations along a track of channel 20 (2)

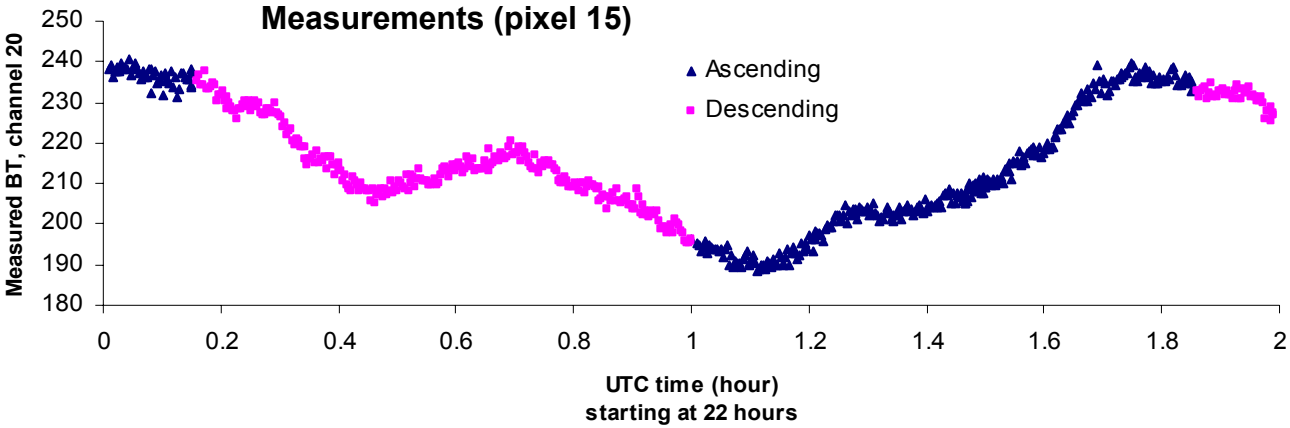

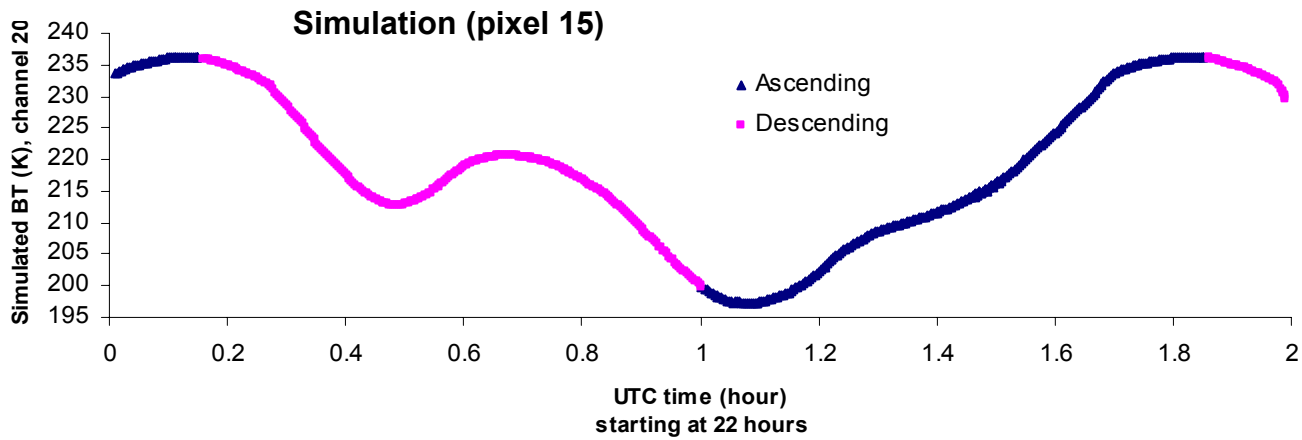

The main features of the measurement time series are well captured by the simulations. The differences are due mainly to the errors of the CIRA profiles used in the simulations.

CIRA profiles: monthly mean, 0 – 120 km, 80ºN – 80ºS every 5º latitude
CIRA: COSPAR International Reference Atmosphere 1986

Zeeman effect case study: measurements and simulations along a track of channel 20 (3)

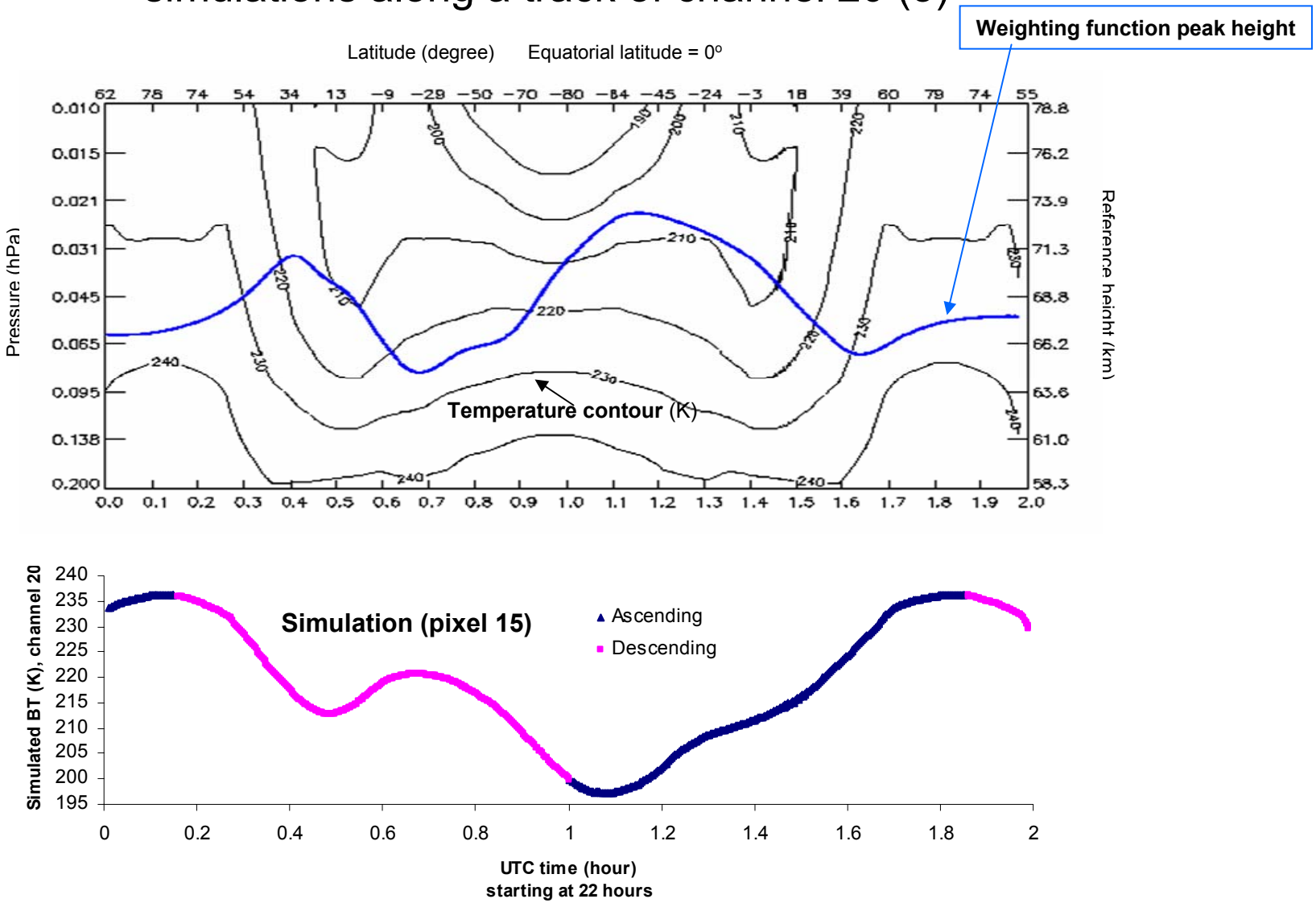

The radiance variation is due to both variations of the weighting function peak height and air temperature

Fast RT Model with inclusion of Zeeman Effect (1)

Algorithm:

(1) Atmosphere is vertically divided into N fixed pressure layers from 0.000076 mb (about 110km) to 200 mb. (currently N=100, each layer about 1km thick).

(2) The Earth's magnetic field is assumed constant vertically

(3) For each layer, the following regression is applied to derive channel optical depth with a left-circular polarization:

$$OD_{lc,i} = c_{i,0} + \sum_{j=1}^{m} c_{i,j} x_{i,j}$$

$x_{i,j}$ – predictors; $c_{i,j}$ - constants

(4) Channel brightness temperature at zenith angle θ is computed as

$$T_{b,lc} = \sum_{i=1}^{n} (\tau_{i-1} - \tau_i) T_{air,i} \quad , \quad \text{where} \quad \tau_i = \tau_{i-1} \exp(-OD_{lc,i} / COS(\theta)), \quad \tau_0 = 1$$

Fast RT Model with inclusion of Zeeman Effect (2)

Training process:

(1) Base line-by-line model: Rosenkranz (1988)

(2) Atmospheric profile set: 48 UMBC profiles extended to 0.000076 mb (about 110 km) by merging them with standard atmospheric profiles

(3) For each profile set, n x m radiances are calculated with n points on B and m points on $COS(\theta_B)$

(4) Zenith angle variation range: 51 - 54

Model test:

(1) Compared with line-by-line model

(a) independent test using 600 TIGR profiles extended to 110 km
(b) independent test using 204 CIRA model profiles
(c) independent test using 52 ECMWF profiles extended to 110 km

(2) Compared with measurements

SSMIS Measurements: data taken on 10/25/2005, 11/15/2005, 2/15/2006, 3/15/2006 and 4/15/2006.
Collocated model input profiles: retrievals collected from the Sounding of the Atmosphere using Broadband Emission Radiometry (SABER) experiment.

Predictors for fast-model layer optical depth

Channel	Predictor
19, 20	ψ, ψB^{-1}, $\cos^2(\theta_B)$,$\psi\cos^2(\theta_B)$, B^{-1}, B^{-2}, $\cos^2(\theta_B)B^2$
21, 22	ψ, $\cos^2(\theta_B)$, B, B^3, $\cos^2(\theta_B)B$, $\cos^2(\theta_B)B^2$
23	ψ, ψ^2, $\cos^2(\theta_B)$, B
24	ψ, ψ^2

ψ – 300/T; T – temperature
B – Earth magnetic field strength
θ_B – angle between magnetic field and propagation direction

Model test (the independent test set was generated from CIRA profiles)

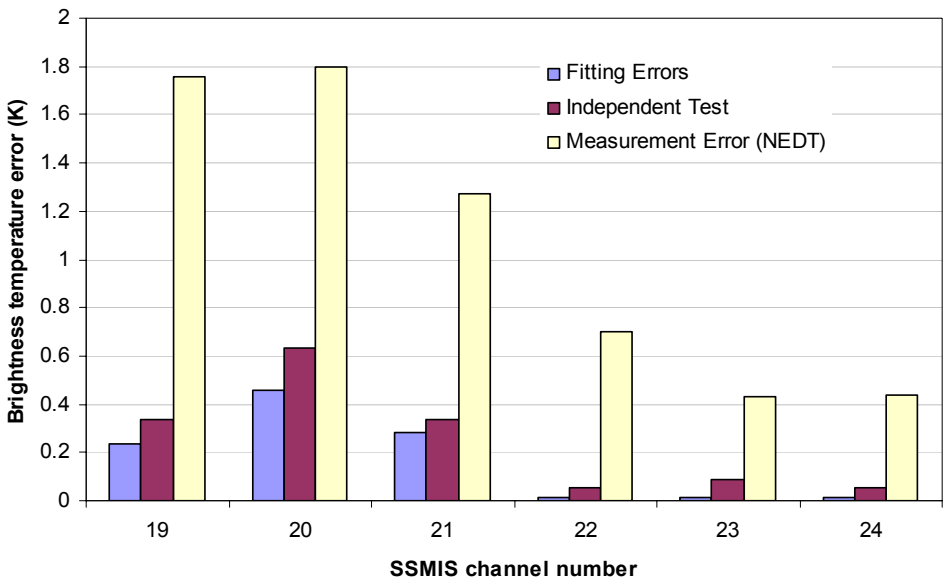

Examples of Jacobian profiles computed with the fast-model's Jacobian routine

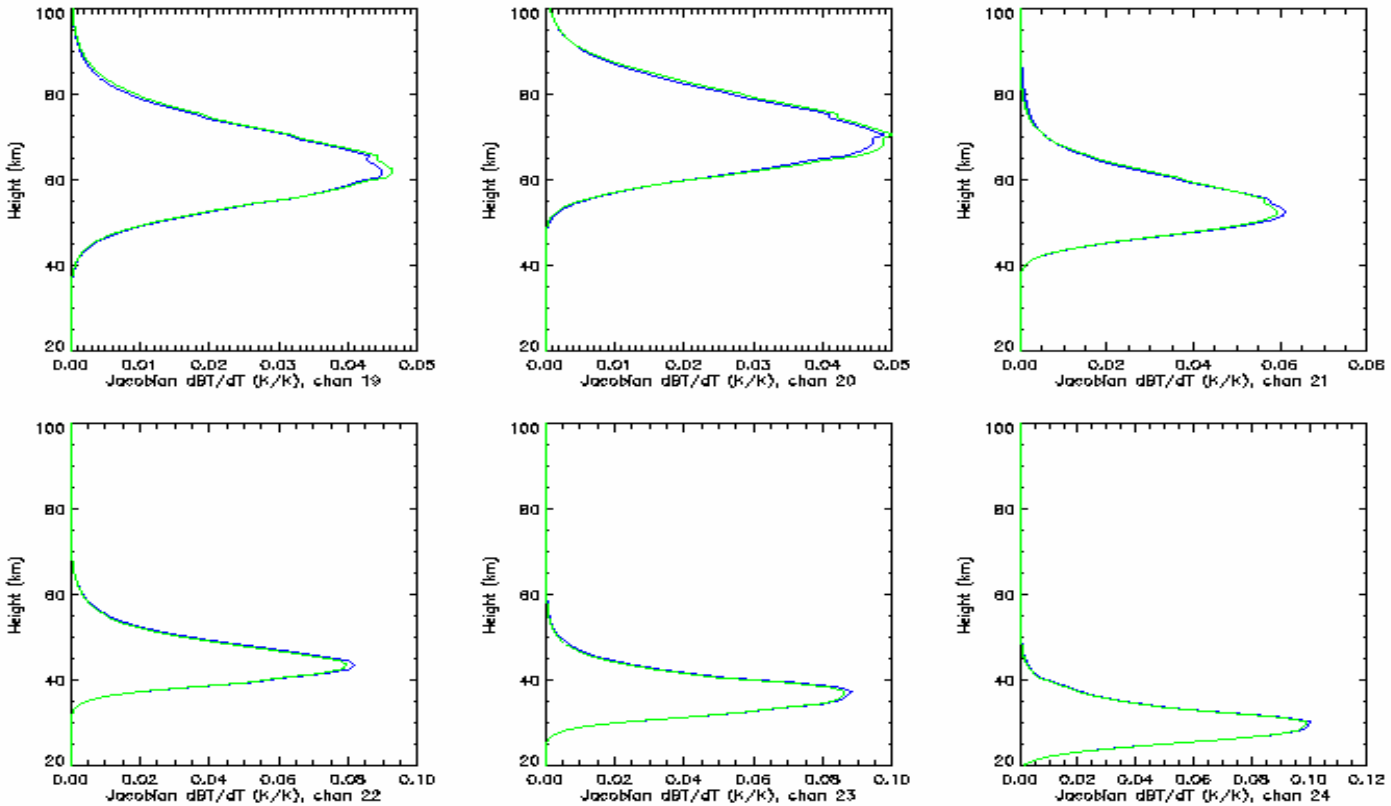

Blue – fast model
Green – finite-difference computed using the line-by-line model

Model results compared with measurements (1097 samples) (1)

	Fast model	Rosenkranz LBL	Liebe93 LBL (line width adjusted with a constant B)
Chan 19	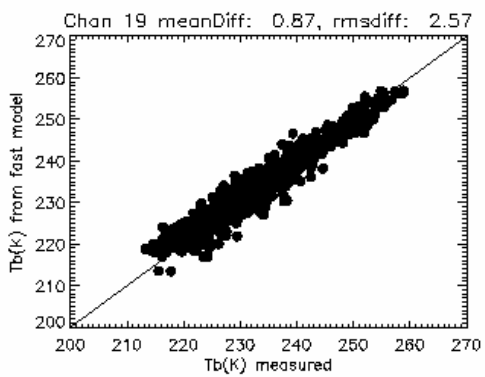	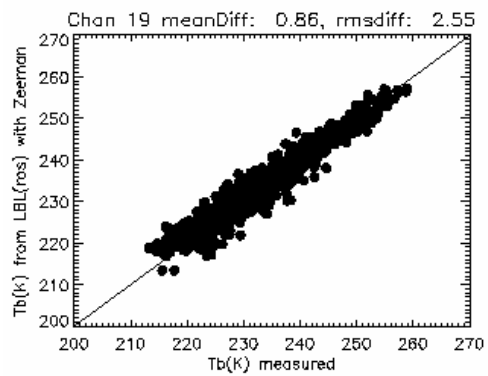	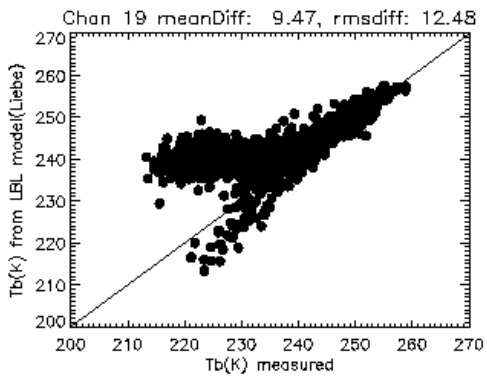
Chan 20	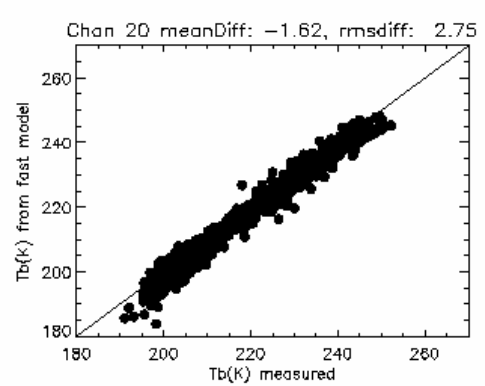	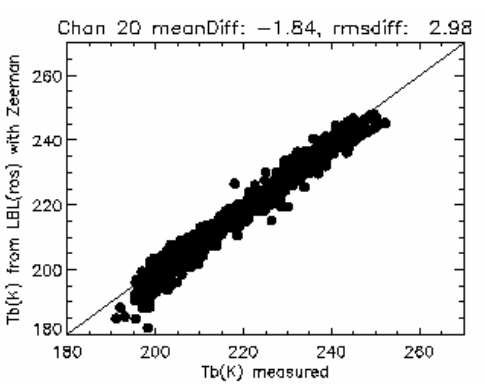	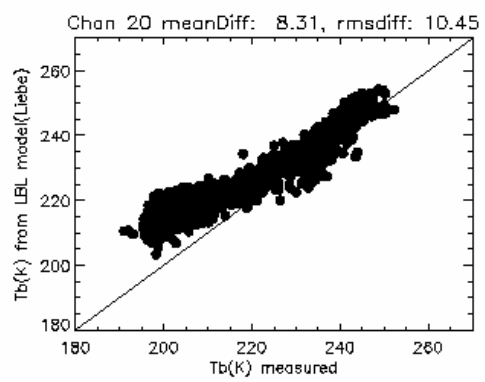
Chan 21	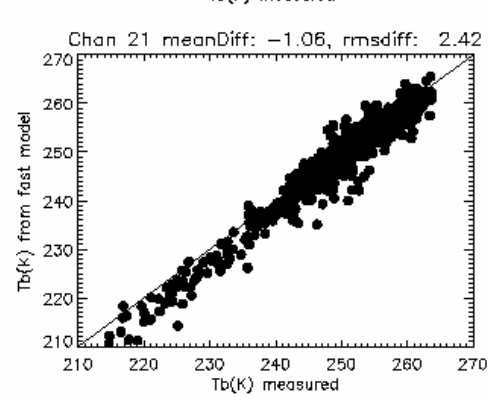	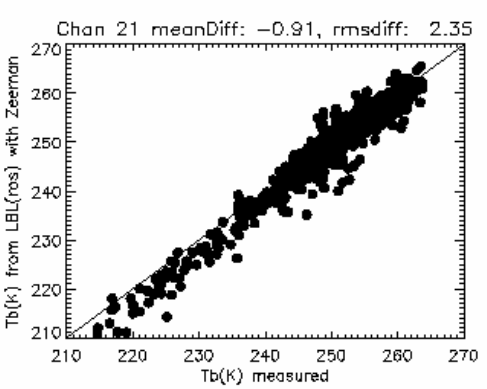	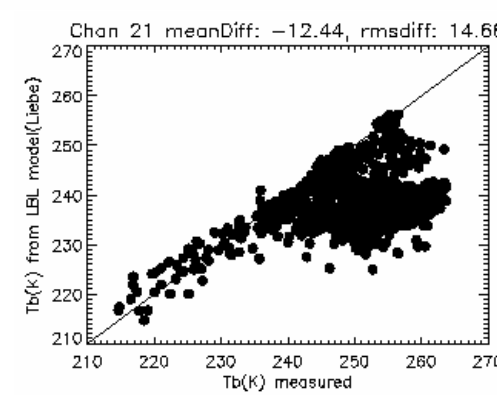

Model results compared with measurements (1097 samples) (2)

	Fast model	Rosenkranz LBL	Liebe93 LBL (line width adjusted with a constant B)
Chan 22	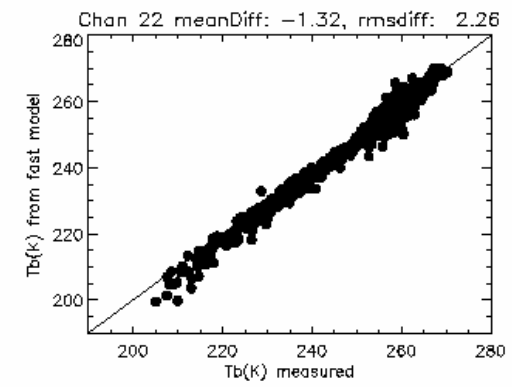	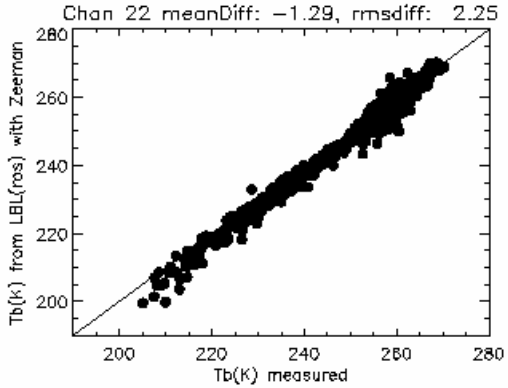	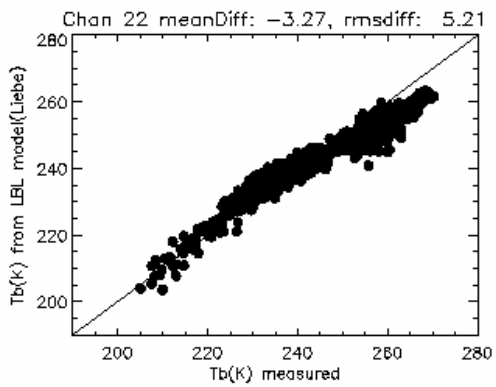
Chan 23	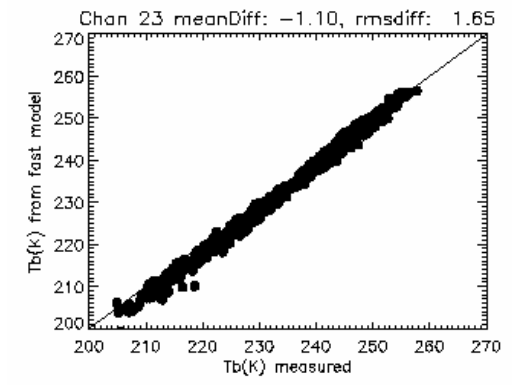	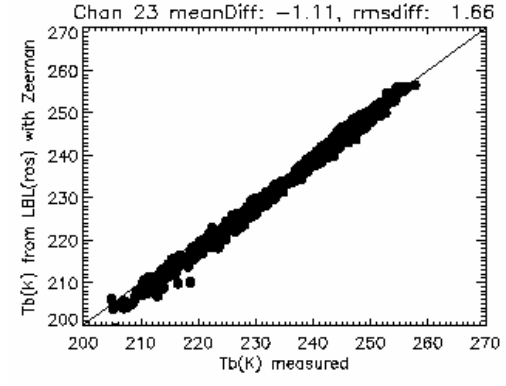	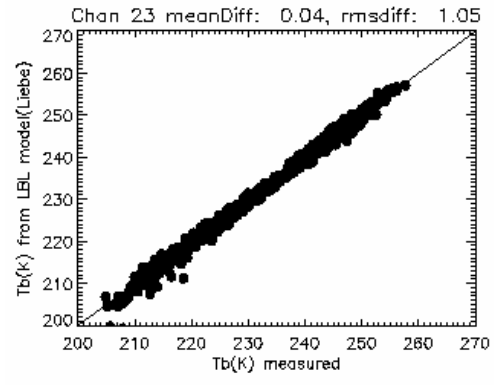
Chan 24	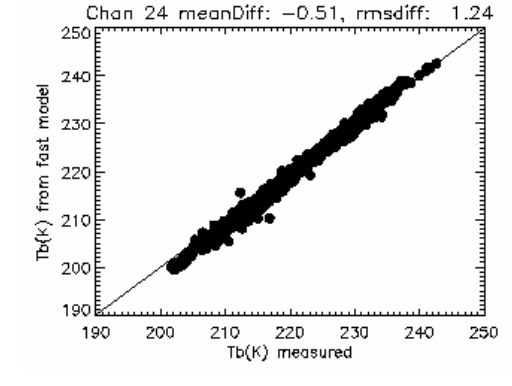	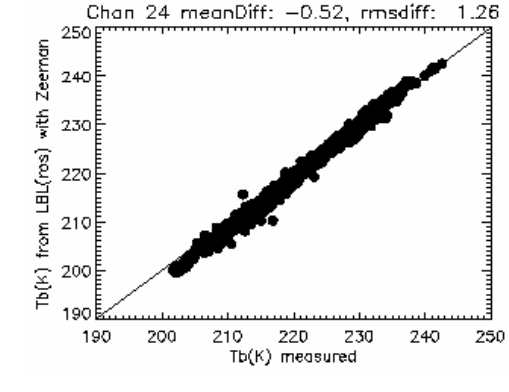	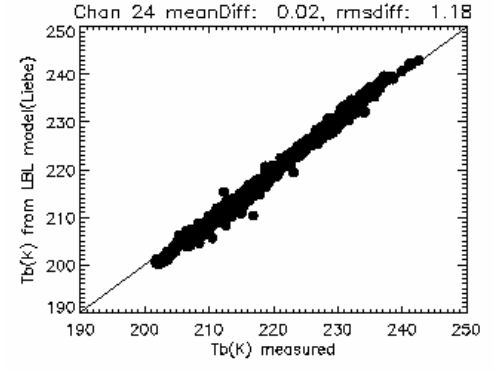

Summary and Conclusions

- A regression-based fast RT model has been developed for both forward and Jacobian calculations; it is based on the Rosenkranz88 line-by-line model and the UMBC 48 profile set.
- The model was tested against the line-by-line model over various independent profile data sets. The RMS differences over the CIRA data set (the worst among the test sets) are 0.34, 0.63, 0.33, 0.053, 0.09 and 0.05 at channels 19 – 24, respectively.
- The model was also compared with the measurements using matched SABER profiles as inputs. Results show that the fast model has performances similar to the line-by-line model in accuracy but a much faster computational speed.
- The weighting function peak heights of the SSMIS channels 19 and 20 decrease with the increase of the Earth's magnetic field strength since the narrow channel passbands are centered at the O2 transition lines and the Zeeman-splitting effect reduces the absorption at the center of the absorption lines.
- The weighting function peak heights of the channels 21 and 22 increase with the increase of the Earth's magnetic field strength since the channel passbands are off the centers of the O2 transition lines and the Zeeman-splitting effect increases the absorption in the wings of the absorption lines.
- The channel radiance calculations are not sensitive to the sign of $COS(\theta_B)$ (radiances at θ_B and $\pi - \theta_B$ have the same value). However, even a slight shift of the channel passband frequencies may make the channel sensitive to the sign.